Feasibility Study of Diagnosing In-Flight Shell Thickness for Laser-Direct-Drive DT Cryogenic Implosions on OMEGA

J. Baltazar,[1,2] R. C. Shah,[1] S. X. Hu,[1,2] K. Churnetski,[1,2] R. Epstein,[1] V. N. Goncharov,[1,2] I. V. Igumenshchev,[1] T. Joshi,[1] W. Theobald,[1,2] and S. P. Regan[1,2]

[1]Laboratory for Laser Energetics, University of Rochester
[2]Department of Mechanical Engineering, University of Rochester

During the deceleration phase of laser-direct-drive inertial confinement fusion experiments, the shell acts as a piston on the fuel, converting its kinetic energy into internal energy of the hot spot and the main fuel. The shell applies a pressure (p_{sh}) on the hot-spot plasma that depends on the in-flight shell thickness (ΔR_i), mass of the shell (M), and velocity of the shell (v), with the relation $p_{sh} \sim \left(M/\Delta R_i^3\right)v^2$ (Ref. 1). The final hot-spot pressure (p_{hs}) scales with the compressive work of the shell, giving $p_{hs} \sim p_{sh}^{5/3}$ [Eq. (62) in Ref. 1]. Many factors in the experiment such as single-beam nonuniformity (laser imprint), target surface debris, and ice roughness, among others, can lead to asymmetric implosions, which perform worse than symmetric implosions. Ablation-surface modulations caused by target features and laser nonuniformity imprint can become the seed for the Rayleigh–Taylor (RT) instability, which further evolves surface modulations at the ablation front during the acceleration phase and decompresses the shell (increases ΔR_i^3), leading to a reduction of the final compression of hot-spot plasma. Surface modulations can be reduced by increasing the shell's entropy, characterized by the shell adiabat $\alpha \sim P/P_F$ and set by the initial picket in the laser pulse (where P_F is the Fermi-degenerate pressure), but there is a trade-off[2] in overall performance. A higher α results in larger ablation velocities and better stability due to increased RT stabilization effects, but with reduced compression achieved in the implosion.[2]

An adiabat study (Refs. 3 and 4), $\alpha \sim 2$ to 6, of plastic-shell implosions using 2-D *DRACO* simulations without laser imprint showed the trend that as the adiabat decreased the shell thickness decreased. When laser imprint was introduced to the 2-D simulations, a decompression of the shell (increase in the shell thickness) was observed and became more prominent as the adiabat decreased due to the decrease in RT stabilization effects. Self-emission measurements taken on OMEGA matched the decompression of the shell observed in the simulations and thus, it was determined that laser imprint explained the decompression of the shell in plastic-shell implosions. A separate adiabat study of DT cryogenic implosions[5] with $\alpha \sim 2$ to 5 using 3-D *ASTER* simulations without laser imprint exhibited a similar trend in the shell thickness to plastic-shell implosions as the adiabat decreased. When laser imprint was introduced to the 3-D *ASTER* low-adiabat ($\alpha \sim 2$) and mid-adiabat ($\alpha \sim 3$) implosions, the shell decompression followed a similar trend to the plastic implosion simulations and measurements. However, measurements of the DT cryogenic implosions did not match the mid-adiabat ($\alpha \sim 3$) implosion simulation; they only matched the low-adiabat implosions ($\alpha \sim 2$). Therefore, it was suggested that additional perturbations or 1-D effects not captured accurately in hydro-simulations may be present in experiments.[5] It is still not clear where the origin of these perturbations occurs; however, some possible sources include the rise of ^{3}He bubbles in the ice layer due to tritium decay, target defects from the cryogenic filing process,[6] and microscopic defects on the ablator surface that were characterized using atomic force microscopy.[7] This motivated an investigation to determine if it was feasible to extend the technique to infer the shell thickness from the self-emission[3,4] of DT cryogenic implosions in order to better understand the effects of laser imprint on shell decompression.

In this work, shell decompression is diagnosed in DT cryogenic implosions from brightness profiles of the coronal plasma and hot-spot emission. Simulations of DT cryogenic implosions are used to study the x-ray signatures for the compressed DT shell. The simulations are post-processed using *Spect3D* to obtain gated images of the x-ray self-emission from the implosion. In experiments,

this is accomplished by recording time-resolved images of x-ray emission from the imploding target using a filtered, 16-pinhole array imager and an x-ray framing camera.[8] The x-ray images are angularly averaged, and the shell thickness is inferred from the separation between the edge of the hot-spot emission and the emission from the outer peak signal, which corresponds with the location of the ablation front. The radial shape from the measurements is dependent on the material of the compressing shell and hot-spot plasma. Therefore, a different analysis is required when analyzing either plastic or cryogenic implosions.

X-ray self-emission measurements of DT cryogenic implosions on OMEGA are simulated using 1-D (*LILAC*) and 3-D (*ASTER*) hydrodynamic codes to study the effects of laser imprint. Metrics for the shell locations were developed by comparing *LILAC* simulations to angularly averaged self-emission profiles.

A 1-D simulation highlighting how the technique is applied to DT cryogenic measurements is shown in Fig. 1. During the acceleration phase, the outer-shell trajectory is obtained by tracking the outer maximum signal point in synthetic gated x-ray images. This signal is blurred by the instrument response function (IRF) and masked by the signal from the hot spot during the deceleration phase; therefore, the trajectory is extrapolated from the acceleration phase to follow a free-fall line in the deceleration phase, where the hot-spot signal has increased and becomes brighter than the signal at the ablation front. The experimental signature for the inner shell turns on after the onset of hot-spot x-ray emission. From comparing the steep gradients in temperature and density from the *LILAC* simulations with the self-emission brightness profiles, it was determined that the inner-shell trajectory is tracked using the 20% intensity from the edge of the hot-spot signal [$I_{20} = 0.20(I_{max}-I_{min}) + I_{min}$]. The 20% intensity point matched the inner-shell location, determined from the hydrodynamic profiles, for different adiabats and target sizes. Taking the difference between the extrapolated and the inner-shell trajectory provides the measurement of the shell thickness over different times.
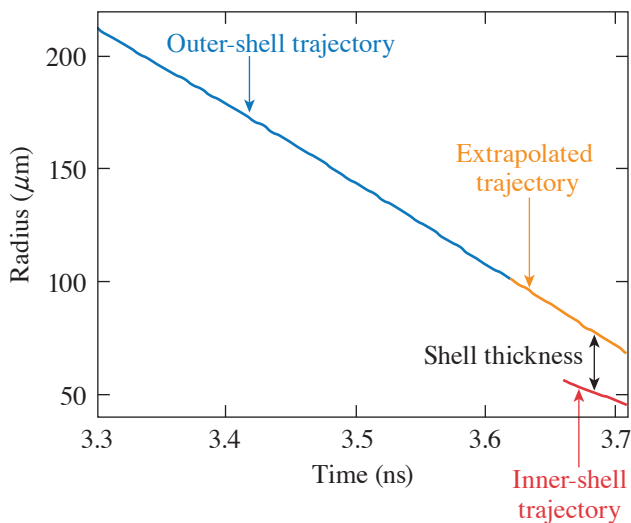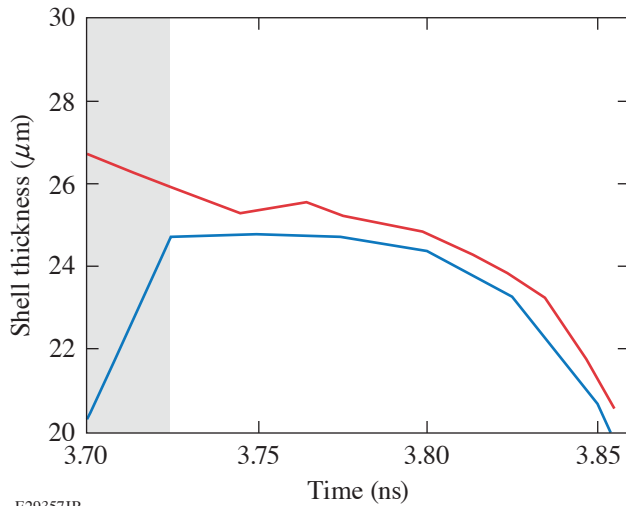

Figure 1

Results from 1-D *LILAC* simulations ($\alpha \sim 2$) and the post-processed (*Spect3D*) measurements show how shell measurements are obtained in the implosion. The outer shell (blue) is tracked using the maximum signal point and is extrapolated to follow a free-fall line (orange) after the laser is turned off. The shell thickness is obtained when the hot spot turns on and the inner-shell (red) trajectory can be tracked.

E29359JR

A comparison of the x-ray–inferred thickness, without applying any spatial or temporal blurring, and the hydrodynamic quantity is shown in Fig. 2. The shell thickness in the 1-D simulation is inferred by tracking the largest gradients in the density profile through measuring the distance between the position of the positive gradient for the inner shell and the negative gradient for the outer shell. In Fig. 2, the gray-shaded region shows that the rebounding shock has not yet collided with the high-density shell. In this time range, the hot spot has not been heated by the shock and the hot-spot emission is low compared to the ablation front. After the shock hits the shell, indicated by the white region in Fig. 2, the hot-spot emission becomes prominent and the x-ray–inferred shell thickness measurements are in agreement with the simulations.

The diagnostic requirements to obtain shell measurements within ~3 μm are ≤10-ps integration and a point spread function with FWHM ≤ 5 μm. The IRF for a pinhole array imager and an x-ray framing camera (20-μm spatial blurring and 40-ps integration), along with other camera parameters, are applied to the synthetic x-ray measurements in Fig. 3 to determine the diagnostic
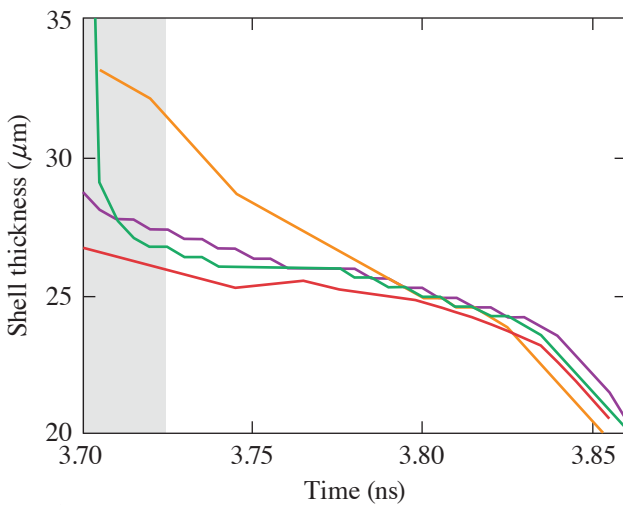
Figure 2
The shell thickness obtained from tracking the hydrodynamic gradients (blue) shows a 1-μm correspondence with shell measurements (without IRF, gray region) after the shock reaches the shell (white region). The temporal and spatial finiteness of the simulations are ~5 ps and ~1 μm, respectively. In the gray region, the rebounding shock has not traversed through the incoming compressing shell; therefore, the emission of the hot spot at this time is low compared to the ablation-front emission.

E29357JR

Figure 3
The x-ray measurement without the IRF is shown by gray shading. Various IRF's were applied to the x-ray measurement to determine the diagnostic requirement: 40-ps integration and 20-μm spatial blurring (orange curve), 10-ps integration and 5-μm spatial blurring (purple curve), and 10-ps integration and 1-μm spatial blurring (green curve). As the spatial and temporal blurring increases the x-ray measurement is affected. The diagnostic requirement (purple curve) followed a similar trajectory to the best-case scenario (without spatial and temporal blurring).

E29675JR

requirements to infer the shell thickness. Applying a temporal blurring of 40 ps showed that the x-ray–inferred shell thickness is increased by ~4 μm but follows the same trajectory as the case without any temporal blurring. Therefore, the measurements are not as sensitive to the temporal blurring compared to the spatial blurring of the instrument. The effect from the spatial blurring has a larger effect on the measurements and leads to a reduction in the inferred shell thickness when the spatial blurring increases, as shown in Figs. 4(a) and 4(b). Application of this technique with the current resolution does not give an accurate measurement of the shell thickness; however, this technique can be used to analyze trends in the shell thickness.

Using the current camera parameters (i.e., a spatial resolution of 20 μm and a temporal resolution of 40 ps) on OMEGA,[9] it was determined that the trend in the shell thickness should be analyzed as opposed to the shell thickness alone. An adiabat study was conducted to demonstrate the effectiveness of the analysis technique on 3-D *ASTER* simulations, with and without laser imprint. A range of shell thickness measurements for implosions of $\alpha \sim 1.7$ to 2.8 is shown in Fig. 5. The low-adiabat ($\alpha = 1.7$) implosion with laser imprint shows a clear increase in the trend when compared with the uniform case, while the high-adiabat ($\alpha = 2.8$) implosion shows only a slight increase in comparison, which is expected due to the higher stability. Additionally, the laser-imprint case of the low-adiabat implosion exhibited an advancement of the hot-spot emission, while the high-adiabat case showed no major discrepancy in the onset of the hot-spot emission. The criteria for the onset of hot-spot emission are defined by the time when the hot-spot signal is ~50% of the peak signal. The early hot-spot emission agrees with a previous analysis of the same campaign[5] and is consistent with what was observed in low-adiabat plastic-shell implosions,[3,4] where the advancement of

the onset of hot-spot emission is caused by the laser-imprint–induced RT instability that causes spikes at the ablation front and bubbles to break through the shell, which drives the inner shell farther toward the center during the acceleration phase. This technique will be applied to experimental data[5] and used to further our understanding of laser imprint on DT cryogenic implosions.
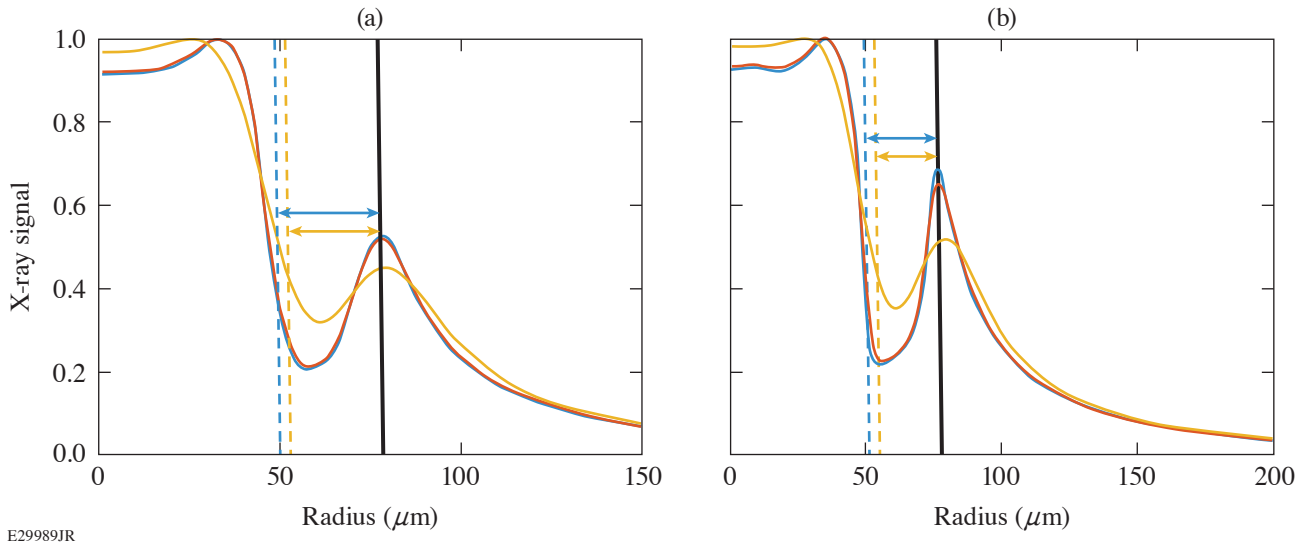
E29989JR

Figure 4
(a) Simulated x-ray brightness profiles obtained in the deceleration phase of a DT cryogenic implosion are shown with an IRF that includes a temporal blurring of 40 ps and a spatial blurring of 1 μm (blue), 5 μm (red), and 20 μm (yellow). The location of the hot-spot boundary was in the same vicinity for the 1-μm and 5-μm cases. Therefore, the location for the hot-spot boundary is shown as dashed lines for the 5-μm (red), and 20-μm (blue) case. (b) Simulated x-ray brightness profiles obtained in the deceleration phase of a DT cryogenic implosion are shown with an IRF that includes a temporal blurring of 10 ps and a spatial blurring of 1 μm (blue), 5 μm (red), and 20 μm (yellow). Increasing the spatial blurring will decrease the inferred shell thickness due to the widening of the diagnosed image of the emission signal profile caused by instrumental effects. Furthermore, the spatial blurring's effect on the measurement is dominant when compared to the effects from the temporal blurring.
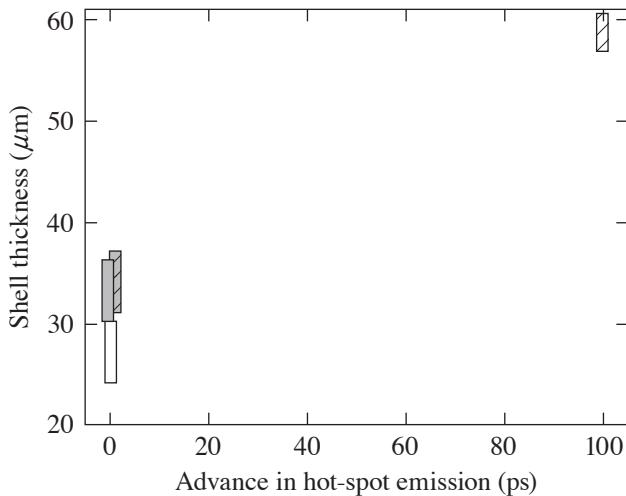

E29676JR

Figure 5
The calculated shell thickness from 3-D *ASTER* x-ray simulations with the IRF of 40-ps temporal resolution and 20-μm spatial resolution for two implosions without (solid color) and with (striped) the effects of laser imprint included: $\alpha = 1.7$ (white box/striped white box) and $\alpha = 2.8$ (gray box/striped gray box). The low-adiabat implosion with laser imprint shows an overall increase in the shell-thickness trend and an advancement in time of the hot-spot emission.[3–5] Both of these characteristics agree with what was observed in plastic-shell implosions. The high-adiabat implosion is less sensitive to the laser-imprint effects and exhibits only a slight increase in the shell thickness and a negligible advancement in time of the hot-spot emission.

1. V. N. Goncharov *et al.*, Phys. Plasmas **21**, 056315 (2014).
2. R. S. Craxton *et al.*, Phys. Plasmas **22**, 110501 (2015).
3. S. X. Hu *et al.*, Phys. Plasmas **23**, 102701 (2016).
4. D. T. Michel *et al.*, Phys. Rev. E **95**, 051202(R) (2017).
5. R. C. Shah *et al.*, Phys. Rev. E **103**, 023201 (2021).
6. I. V. Igumenshchev *et al.*, Phys. Plasmas **20**, 082703 (2013).
7. S. P. Regan *et al.*, Nucl. Fusion **59**, 032007 (2019).
8. D. K. Bradley *et al.*, Rev. Sci. Instrum. **63**, 4813 (1992).
9. A. K. Davis, "Laser Ablation and Hydro-Efficiency of Capsules Imploded in a Direct-Drive Inertial-Confinement-Fusion Configuration," Ph.D. thesis, University of Rochester, 2017.